

PKS B1400–33: an unusual radio relic in a poor cluster

Ravi Subrahmanyam

Australia Telescope National Facility, CSIRO, Locked bag 194, Narrabri, NSW 2390, Australia

A. J. Beasley

Owens Valley Radio Observatory, California Institute of Technology, Pasadena, CA 91125

W. M. Goss and K. Golap

National Radio Astronomy Observatory, PO Box 0, Socorro, NM 87801

R. W. Hunstead

School of Physics, University of Sydney, NSW 2006, Australia

ABSTRACT

We present new arcminute resolution radio images of the low surface brightness radio source PKS B1400–33 that is located in the poor cluster Abell S753. The observations consist of 330 MHz VLA, 843 MHz MOST and 1398 and 2378 MHz ATCA data. These new images, with higher surface brightness sensitivity than previous observations, reveal that the large scale structure consists of extended filamentary emission bounded by edge-brightened rims. The source is offset on one side of symmetrically distributed X-ray emission that is centered on the dominant cluster galaxy NGC 5419. PKS B1400–33 is a rare example of a relic in a poor cluster with radio properties unlike those of most relics and halos observed in cluster environments.

The diffuse source appears to have had an unusual origin and we discuss possible mechanisms. We examine whether the source could be re-energized relic radio plasma or a buoyant synchrotron bubble that is a relic of activity in NGC 5419. The more exciting prospect is that the source is relic plasma preserved in the cluster gaseous environment following the chance injection of a radio lobe into the ICM as a result of activity in a galaxy at the periphery of the cluster.

Subject headings: galaxies: clusters — radio continuum: galaxies — radio sources: general, diffuse

1. Introduction

Extended emission structures with steep radio spectral indices, which are not obviously associated with any optical galaxy, are sometimes observed in rich cluster environments. These sources are broadly separated into cluster wide ‘halos’ that appear relaxed and symmetric with respect to the X-ray intracluster gas, and the peripheral arc-like structures referred to as ‘relics’. Both types are predominantly observed to be associated with hot ($T_X \geq 6$ keV), X-ray luminous ($L_X > 4 \times 10^{44}$ erg s $^{-1}$) rich compact clusters (Schuecker and Böhringer 1999); however, the clusters that have peripheral relics may have somewhat lower temperatures (Feretti 1999). A standard hypothesis is that these sources are relic synchrotron plasma that has been revived.

PKS B1400–33 is an extended radio source, with an 85 MHz flux density of 57 Jy (Mills, Slee and Hill 1960), and has the lowest surface brightness of any source in the Parkes catalog. PKS B1400–33 appears to be associated with the poor cluster S753 of Abell richness class 0; however, the source not been conclusively identified with any optical galaxy. Previous low frequency images of the source using the VLA and the MOST (Goss et al. 1987) showed a relatively bright rim along the NE edge and low surface brightness filamentary emission trailing off to the SW. The source was observed to have a steep spectrum with spectral index α ($S_\nu \propto \nu^{-\alpha}$) in the range 1.2-2.4.

The unusual nature of this possible relic radio source and its potential value as a probe of the gas dynamics and evolution of poor cluster environments has led us to carry out new radio observations of the source. We have made images with improved surface brightness sensitivity at 330 MHz using the Very Large Array (VLA), at 843 MHz with the Molonglo Observatory Synthesis Telescope (MOST) and at 1398 and 2378 MHz using the Australia Telescope Compact Array (ATCA). Table 1 is a summary of the new radio observations. These are presented here followed by discussions on the origin of this source in the light of the current understanding of the phenomenology and formation of relics in the intracluster medium (ICM).

2. The radio continuum images

PKS B1400–33 was observed at 330 MHz with the VLA separately in the CnB, C, and DnC array configurations in order to image the extended emission in this low surface brightness source. Hybrid arrays were included because of the southern declination. The data were self calibrated and imaged in AIPS using three-dimensional imaging routines. The VLA 330 MHz image of the source is shown in Fig. 1. The image has been made combining

data from all the configurations with a beam of FWHM 77×53 arcsec 2 at a P.A. of -24° ; the r.m.s. noise is 2.5 mJy beam $^{-1}$. This radio image, as well as all the higher frequency radio images presented here, has been corrected for the primary beam attenuation.

Because of its steep spectrum, the total extent of the diffuse source is best defined by the 330 MHz VLA image. The low surface brightness source is bounded to the NE by a relatively bright rim of emission (marked NE rim in Fig. 1), while the source is bounded on the opposite SW side by a second fainter ridge of emission (marked SW rim in Fig. 1). Both the bounding rims are concave outwards. The emission that lies between the bounding ridges is filamentary and decreases in surface brightness from NE towards the SW. The bright compact source that is observed in the image close to the NW edge of the extended source, at RA $14^h03^m38\rlap{.}^s7$, DEC $-33^\circ58'39''$ (J2000.0), has a flux density of 0.95 Jy at 330 MHz; the compact source appears slightly resolved and has a deconvolved size of about 25 arcsec. As discussed below, this compact component is identified with the galaxy NGC 5419. There is evidence for a protrusion towards the SW beyond the bounding rim; this extension, marked P in Fig. 1, is observed in the 330 MHz image at a level of ~ 20 mJy beam $^{-1}$. The total flux density of the extended radio source PKS B1400–33 is 8.5 Jy at 330 MHz, excluding the emission from NGC 5419 and the source $5.5'$ to its south, marked B in Figs. 1–4, that is presumably an unrelated confusing source. The error in the absolute flux density scale at 330 MHz is believed to be about 2 %.

The 843 MHz MOST image of PKS B1400–33 is shown in Fig. 2. This image, obtained using the most sensitive $23'$ field of view, better reproduces the extended structure than the 843 MHz image in Goss et al. (1987). The image has been made with a beam of FWHM 77×43 arcsec 2 at a P.A. of 0° and has an r.m.s. noise of 1 mJy beam $^{-1}$. The 843 MHz image of the extended source shows the relatively bright rim along the NE, the filamentary structures trailing from this ridge towards the SW and the curved rim that defines the boundary of the diffuse source at the SW end. The flux density of the extended source (again excluding NGC 5419 and the embedded background source B) is 1.3 Jy at 843 MHz. NGC 5419 has a flux density of 0.46 Jy at 843 MHz. Additionally, the 843 MHz image clearly reveals a local emission peak embedded within the diffuse emission at RA $14^h03^m55\rlap{.}^s9$ DEC $-34^\circ06'03''$ (J2000.0); we hereinafter refer to this feature as component C. It has a flux density of 13 mJy beam $^{-1}$ at 843 MHz. The flux density scale in the MOST image is accurate to 5 %.

PKS B1400–33 was observed using the 375 m and the 750B 750 m array configurations of the ATCA during 1995 Jan and June. Observations were made in two 128 MHz wide bands centred at 1398 and 2378 MHz; the bands were covered using 13 channels. The extended source was covered with a nine-pointings mosaic with the pointings spaced $8'$ apart in RA and DEC. Continuum images at the two frequencies were made separately using

the channel data, adopting a bandwidth synthesis approach to avoid bandwidth smearing effects; the mosaic imaging was carried out in AIPS++. Deconvolution used the multi-scale CLEAN algorithm: the bright compact source at the edge of the extended emission was first removed from the ‘dirty’ image using a ‘box’ CLEAN and subsequently a multi-scale CLEAN was performed on the residual image. The final images at the two frequencies were then convolved to identical beams of FWHM 70×45 arcsec 2 at a P.A. of 0°. Consequently, different weightings were adopted at the two ATCA frequencies during the imaging step; however, the convolution to identical final beams implies that the images presented here effectively have the same visibility range. ATCA mosaic images of the PKS B1400–33 field at 1398 and 2378 MHz are shown in Figs. 3 and 4 respectively. The r.m.s. noise is 0.5 mJy beam $^{-1}$ in both images. The relatively bright ridge along the NE and the filamentary emission trailing towards SW have been imaged at 1398; however, at 2378 MHz, the ridge appears non-uniform and clumpy and the filamentary emission is undetected, possibly due to the poorer signal-to-noise ratio. The bounding ridge at the SW of the extended source is not detected in either of these higher frequency ATCA images. The wide-field mosaic images show several continuum sources, presumably unrelated, in the field. Based on the ATCA data, the flux density of NGC 5419 is 0.30 and 0.23 Jy at 1398 and 2378 MHz respectively. The total flux density of the extended source PKS B1400–33 is 0.46 and 0.10 Jy at 1398 and 2378 MHz. The central component C is detected in both the ATCA images with flux density 5 and 2 mJy beam $^{-1}$ at 1398 and 2378 MHz respectively. The absolute flux density scale in the ATCA observations was set using observations of PKS B1934–638 whose flux density is known, relative to sources in the northern hemisphere, with an uncertainty of 2 %.

The parameters of the radio images presented here are in Table 2. PKS B1400–33 has an angular size of approximately $24' \times 14'$. Assuming that the source is at the distance of the cluster S753, which is $40h^{-1}$ Mpc from the Sun ($h = H_0/100$, where H_0 is the Hubble constant in km s $^{-1}$ Mpc $^{-1}$), the linear dimensions of the extended source are approximately $280h^{-1}$ kpc $\times 160h^{-1}$ kpc. The 1.4 GHz radio luminosity of the extended source is $2.2h^{-2} \times 10^{22}$ W Hz $^{-1}$.

3. The distribution of the radio spectral index

The radio spectra of the extended emission and of the compact source associated with NGC 5419 are shown in Fig. 5. Apart from the measurements at 330, 843, 1398 and 2378 MHz reported here, the plot includes previous estimates of the flux densities of the compact and extended sources in Goss et al. (1987) as well as our estimates of the 85 and 408 MHz

flux densities of the extended source that are based on the measurements made by Mills, Slee and Hill (1960) and Bolton, Gardner and Mackey (1964) and extrapolations of the flux density of NGC 5419 to low frequencies.

The extended radio source PKS B1400–33 (not including NGC 5419 and the background source B) has a mean spectral index $\alpha = 2.0$ between 330 and 1398 MHz. The spectral index appears to steepen to $\alpha = 2.9$ between 1398 and 2378 MHz; this may be because of missing extended flux density in the 2378 MHz interferometric mosaic image. The 85 MHz data indicates a spectral flattening at low frequencies. Our measurements of the flux density of the compact source associated with NGC 5419 are consistent with previous estimates; the compact source has a spectral index $\alpha = 0.8$. The compact source B located 5'5 south of NGC 5419 has $\alpha = 0.8$ between 843 and 1398 MHz and $\alpha = 1.0$ between 1398 and 2378 MHz.

The images at 330 and 843 MHz were convolved to a final beam of 80" FWHM and the distribution of the spectral index, that was computed from these images, is shown in Fig. 6. Effectively, the two images used for computing the spectral index image have the same u,v-coverage. Towards the NE ridge α is 1.3–1.4 and towards the SW rim at the opposite end of the diffuse source α is 1.6–1.7. In the region between the two rims, α is 1.7 towards component C whereas the spectral index is steeper, with α in the range 1.8–2.4, over most of the filamentary emission.

Between 1398 and 2378 MHz, the spectral index of the NE ridge is 1.9 and this is steeper than the spectral index between 330 and 843 MHz. Component C, which is detected in both the 1398 and 2378 MHz images, has a spectral index of $\alpha = 1.7$ at these frequencies, similar to that between 330 and 843 MHz.

4. The optical galaxy environment

The 330 MHz radio contours are overlaid on a DSS digitization of the UK Schmidt optical image of the field in Fig. 7. The bright compact radio source is coincident with the galaxy NGC 5419 which is the dominant galaxy of a cluster listed in the supplementary catalog of Abell, Corwin and Olowin (1989) as S753. This is a poor cluster of Abell richness class 0. Willmer et al. (1991) find that the mean harmonic radius (Maia, da Costa and Latham 1989) of the cluster members is $1.26h^{-1}$ Mpc. This radius corresponds to an angular size of 1°8. The extended source PKS B1400–33 is located well within the cluster radius; however, the source is offset to one side of the central dominant galaxy. Herein we assume that PKS B1400–33 is at the distance of S753. S753 has a high spiral content (45

(%) and a low velocity dispersion of 416 km s^{-1} (Willmer et al. 1991). Using different criteria for cluster membership, Fadda et al. (1996) estimate the cluster internal velocity dispersion to be 536 km s^{-1} .

In the DSS optical image, there are no detectable optical counterparts that are positionally coincident with either the compact radio source 5'5 to the south of NGC 5419 or the central component C.

5. The thermal gaseous environment

The cluster is estimated to have a virial mass of $1.5 \times 10^{14} \text{ M}_\odot$ (Willmer et al. 1991). Based on the velocity dispersion - temperature relation given by Bird, Mushotzky and Metzler (1995), we estimate that isothermal X-ray gas in the relatively low-depth potential well would have a temperature of 2–3 keV. A 3 ks PSPC pointed observation of the S753 cluster was recovered from the ROSAT archives. We have examined the 0.1–2.4 keV broad-band image of the cluster. There is a bright peak in the X-ray emission at the location of NGC 5419, which might be emission associated with the interstellar medium of the central galaxy or a result of a cooling flow. There is a secondary peak, located about 3'6 to the west, that does not appear to be associated with any cluster member. To detect any low surface brightness diffuse X-ray emission (in the presence of the strong unresolved sources), we convolved the 15" pixel counts on the sky image with a Gaussian of FWHM 1' followed by a box-car of width 2'. A contour representation of this X-ray image is shown in Fig. 8 overlaid on greyscales of the 330 MHz VLA image. A low surface brightness extended X-ray halo component is observed, centered on NGC 5419, with a radius of 16' ($190h^{-1} \text{ kpc}$). The X-ray halo appears to surround the radio source PKS B1400–33. There is no evidence in this ROSAT image for any deficit or excess of X-ray emission towards the extended radio source. The X-ray properties of S753 are typical of poor groups (Mulchaey and Zabludoff 1998), where the X-ray emission is dominated by a component associated with a bright cluster member.

6. The anomalously low surface brightness of PKS B1400–33

The physical parameters in those powerful FR II radio galaxies and head-tail and wide-angle tail radio sources, which have extended emission structures much bigger than the size of the host galaxy, may be useful probes of the surrounding medium (Feretti, Perola and Fanti 1992; Subrahmanyan and Saripalli 1993). The radio structures that are overpressured with respect to the ambient medium expand in the ambient gas with speeds limited by ram

pressure; therefore, derivations of the ambient gas properties depend on a knowledge of the expansion speeds. Radio structures with relatively low surface brightness, like the diffuse source PKS B1400–33, potentially have the lowest internal energy densities and pressures, and are most likely to be in a static pressure balance with the ambient thermal gas. Therefore, the internal state of such synchrotron plasma might be a direct probe of the surrounding thermal environment.

Subrahmanyam and Saripalli (1993) studied the properties of the synchrotron plasma in the diffuse bridges of the lobes of powerful and giant radio galaxies located in the field. These structures, which lie outside cluster environments and outside the ubiquitous thermal halos of the host ellipticals, are among the lowest surface brightness radio components outside clusters. These giant bridges have 1 GHz surface brightness $\sigma_{1 \text{ GHz}} \approx 0.2 \text{ Jy arcmin}^{-2}$ (Subrahmanyam, Saripalli and Hunstead 1996) and the pressure inferred for the synchrotron plasma, assuming minimum energy conditions (Miley 1980), is $p_e = 1-2 \times 10^{-14} \text{ dyne cm}^{-2}$. A study of the internal pressures in the low surface brightness tails of tailed radio galaxies in Abell clusters (Feretti, Perola and Fanti 1992) shows that in cluster environments p_e exceeds $10^{-13} \text{ dyne cm}^{-2}$. The higher pressures inferred for the radio galaxies in clusters are consistent with the relatively higher ambient densities and temperatures in the intracluster medium.

Diffuse cluster radio sources, which cannot be identified with any active radio galaxy, have a wide range in their surface brightness and p_e in the range $10^{-14}-10^{-13} \text{ dyne cm}^{-2}$ (Feretti 2002). Among these sources, the peripheral relics, like the arcs in A3667 (Röttgering et al. 1997), have $\sigma_{1 \text{ GHz}}$ a factor 10 larger than the giant bridges in the field and in this respect they are similar to the tailed radio sources in cluster environments; however, the peripheral relics have been inferred to have a wide range in their p_e (see, for example Feretti and Giovannini (1996)). The lowest surface brightness radio components in cluster environments are the diffuse cluster wide halos. Coma C, a prototypical example of such a halo, has $\sigma_{1 \text{ GHz}} \approx 3 \text{ mJy arcmin}^{-2}$ (Kim et al. 1990) and an inferred $p_e \approx 8 \times 10^{-15} \text{ dyne cm}^{-2}$ (Giovannini et al. 1993). Other cluster halo sources are inferred to have a similar low $p_e \lesssim 10^{-14} \text{ dyne cm}^{-2}$ (Feretti and Giovannini 1996). The extremely low synchrotron plasma pressure inferred for the halo sources appears inconsistent with their location at the centers of rich clusters. This anomaly might be related to the origin of the halo: the diffuse halos are not identified with any currently active galaxy and are, instead, postulated as being reaccelerated relic plasma (Brunetti et al. 2001). The halos are believed to have an origin different from the peripheral relics.

The surface brightness of PKS B1400–33 is about $3 \text{ mJy arcmin}^{-2}$ at 1 GHz. If we assume that the cm-wavelength spectrum of PKS B1400–33 continues with $\alpha = 2.0$ to low

frequencies, the inferred p_e is 1×10^{-13} dyne cm $^{-2}$. However, Mills, Slee and Hill (1960) measured the 85 MHz flux density of the source to be 57 Jy giving the source a mean spectral index of $\alpha = 1.4$ between 330 and 85 MHz. This indicates that the spectrum has a break somewhere in the range 0.1–0.3 GHz and that the spectral index flattens towards lower frequencies. Assuming a spectral break at 165 MHz with $\alpha = 0.7$ below the break and $\alpha = 2.0$ above, we infer $p_e = 5 \times 10^{-14}$ dyne cm $^{-2}$.

PKS B1400–33 appears to be in a poor cluster environment, where the ambient gas pressure is probably higher than that surrounding the bridges of giant radio galaxies in the field. The cluster in which PKS B1400–33 is located has a relatively low inferred gas temperature, a low X-ray luminosity, and the ambient environment is not as extreme as that in rich clusters. PKS B1400–33 has an extremely low surface brightness very similar to that of cluster wide halo sources such as Coma C. However, unlike the halo sources, PKS B1400–33 is not centrally located in the cluster. Additionally, halos are almost exclusively found in rich clusters with high velocity dispersions, whereas the cluster environment of PKS B1400–33 is poor. The p_e in PKS B1400–33 is higher than that in giant bridges in the field as well as diffuse halo sources in cluster centers, but it is not as high as that in tailed radio sources in rich clusters. The intermediate value for p_e is consistent with PKS B1400–33 being a relic in a poor cluster environment; however, the surface brightness is relatively low as compared to typical relicts.

Rood #27 (Harris et al. 1993) is another low surface brightness source in a poor galaxy environment. This diffuse source is not obviously identified with any optical galaxy and appears to be a relic. Rood #27 also has an extremely low $\sigma_{1 \text{ GHz}}$ but somewhat higher than that of PKS B1400–33; additionally, the spectral index of Rood #27 is close to 0.6 and is not as steep as that of PKS B1400–33.

7. On the nature of the unusual source PKS B1400–33

The extremely steep spectral index (mean $\alpha = 2$) of PKS B1400–33 suggests that the source is composed of relic synchrotron plasma in which energy injection has ceased and, subsequently, the spectral index has steepened as a consequence of synchrotron losses (spectral aging). The steep spectrum indicates that there is no on-going or recent reacceleration. Moreover, the steep spectrum also suggests that the emissivity of this source has not been significantly enhanced as a result of adiabatic compression. PKS B1400–33 is likely a relic of a source that was bright in its youth. Extrapolating the measured flux density of 57 Jy at 85 MHz to cm wavelengths using a spectral index of $\alpha = 0.7$, we infer that the source would have had a 1 GHz flux density at least 10 Jy prior to any losses. The radio power would

have exceeded 4×10^{24} W Hz $^{-1}$ at 1 GHz and PKS B1400–33 would have been a powerful radio source.

Our estimate that the diffuse source has a p_e in the range $5\text{--}10 \times 10^{-14}$ dyne cm $^{-2}$ implies that the equipartition magnetic field is 1–2 μ G and spectral aging is predominantly via inverse Compton losses against the cosmic microwave background. If we assume that the diffuse source was initially created radiating with a power law spectrum and with spectral index $\alpha < 2$, and that the electrons with higher Lorentz factors were depleted as a consequence of spectral aging, the spectral break would move below 300 MHz in about 10 8 yr. If, today, the break is at 165 MHz, the source age is 5×10^8 yr.

7.1. A relic created by NGC 5419?

PKS B1400–33 has a radio power $0.9 \times 10^{23}h^{-2}$ W Hz $^{-1}$ at 1.4 GHz; before any spectral aging the radio power may have been higher. Luminous ellipticals with absolute magnitudes $M_R \lesssim -21$ are usually the hosts of extended radio sources with these high radio powers (Ledlow 1997). It follows that the host galaxy of PKS B1400–33 ought to be a bright elliptical with $m_R \lesssim 13.5$ (assuming $h = 0.5$). 11 E/S0 galaxies listed by Willmer et al. (1991) to be in S753 are of this magnitude and NGC 5419 is the most luminous.

NGC 5419 is a bright radio source suggesting that the central engine in the galactic nucleus is currently active. However, based on Fig. 7, NGC 5419 is located just outside the boundary of the extended source. Moreover, as seen in Figs. 2 and 3, there is an emission gap between the compact source associated with the galaxy and the extended source. Finally, the portion of the extended source closest to the galaxy has a different spectral index ($\alpha = 1.6$) compared with the compact source ($\alpha = 0.8$). Additionally, there is no evidence for any spectral index gradient away from NGC 5419.

Nevertheless, it might be that the extended source PKS B1400–33 is a relic of past activity in NGC 5419. In this case, the displacement of the extended structure from NGC 5419 could be due to Rayleigh Taylor instability of the light relic synchrotron plasma embedded in a denser X-ray gaseous environment and at the bottom of the cluster potential well (Churazov et al. 2000). Simulations of the rise of such buoyant bubbles (Churazov et al. 2001) indicate that the plasma may initially deform into a torus as it rises and later form pancake-like sheets at altitudes where the densities of the two-phase medium attain equilibrium. The arc-like boundaries of PKS B1400–33 might be fragments of such a global toroidal structure viewed in projection. In this scenario, the relatively flatter spectrum component C embedded in the diffuse source might be the past site of nuclear activity.

The ‘ghost’ cavities that are observed in the Perseus cluster (Fabian et al. 2000) and in Abell 2597 (McNamara et al. 2001), are believed to be relic synchrotron bubbles. Buoyancy has been proposed as the mechanism for their displacement from the centers of the clusters. If PKS B1400–33 has been displaced from NGC 5419 over the distance of $r = 100h^{-1}$ kpc by buoyant forces, we would expect the movement to occur over a timescale

$$t_b \approx \sqrt{(\rho_e/\rho_{ICM}) \times (r^3/GM(< r))}, \quad (1)$$

where ρ_e is the density of the entrained thermal matter, ρ_{ICM} is the density of the thermal intra-cluster medium and $M(< r)$ is the gravitational mass of the cluster within radius r . We infer that $M(< 100h^{-1}$ kpc) $\sim 7.5 \times 10^{10}$ M_\odot from the cluster parameters derived by Willmer et al. (1991) and, consequently, the timescale of the buoyant motion $t_b < 1.6 \times 10^9$ yr. If we assume that the motion takes place in the spectral aging timescale of 5×10^8 yr, we infer that the ratio of ambient to entrained thermal material is $(\rho_{ICM}/\rho_e) \approx 10$.

Alternatively, we consider the possibility that the displacement between PKS B1400–33 and NGC 5419 is the result of transverse motion of the galaxy itself. Assuming a timescale of 5×10^8 years and a separation $r = 100h^{-1}$ kpc, the implied transverse velocity is $190h^{-1}$ km s $^{-1}$. This is consistent with the cluster velocity dispersion and with the peculiar radial velocity of NGC 5419 of 184 km s $^{-1}$ (Willmer et al. 1991). The central component C, which has a relatively flatter spectrum, might be the site where the galaxy was situated when activity in its nucleus created the extended source.

In the above scenario, PKS B1400–33 was created in the past owing to nuclear activity in NGC 5419. Subsequently, the activity ceased, and the current nuclear activity in NGC 5419 is a new activity phase. The compact radio source associated with NGC 5419 has a spectral index $\alpha = 0.6$ that is flatter than that observed in the extended emission; this gradient is consistent with the hypothesis of restarting activity (see, for example, Roettiger et al. (1994)). If the spectral age derived for PKS B1400–33 is nearly the true age of the relic source, it follows that the nuclear activity in NGC 5419 has restarted in less than 5×10^8 yr. It may be noted that McNamara et al. (2001) derived a timescale of 10^8 yr for recurrent outbursts in the central source of Abell 2597.

7.2. Relic synchrotron plasma re-energized by shocks in the ICM?

Clusters of galaxies are believed to be dynamically evolving at the present epoch, accreting mass components and undergoing mergers, which result in ICM gas density discontinuities that are either shock fronts or cold fronts (Forman et al. 2002). Relic radio sources

that have been rendered invisible at cm wavelengths owing to synchrotron losses might be present in the intergalactic medium (Ensslin 1999). Ensslin et al. (1998) have proposed that PKS B1400–33 may be relic plasma in which the particles have been reaccelerated by the passage of shocks related to the cluster evolution. In this model, PKS B1400–33 may have an origin external to S753.

Steep spectrum relics are preferentially found at the peripheries of relatively rich clusters usually with arc-like morphologies. Examples are the peripheral arc-like source J1324–3138 in A3556 (Venturi et al. 1999) and the arcs in A3667 (Röttgering et al. 1997), located on two opposite sides of the cluster center with no detection of any diffuse extended emission between. PKS B1400–33 does indeed have edge-brightened arcs; however, in this case there is diffuse filamentary emission between and, additionally, the entire source is on one side of the cluster center.

The morphological peculiarities in this relic might be a result of an unusual projection geometry. However, the parent cluster S753 has a shallow gravitational potential well and the ICM presumably has a relatively low gas pressure. Consequently, relativistic electrons that are distributed over a wider area in the relic plasma may survive radiative losses and be available to be re-energized by a passing shock wave (Ensslin and Brüggen 2002). The steep spectral index of PKS B1400–33 (mean $\alpha = 2$) implies a relatively low shock compression ratio $R = 2$; this is consistent with the flatter gravitational potential of the poor cluster. Simulations of the passage of a shock across a hot magnetized bubble (Ensslin and Brüggen 2002) suggest that the relic may transform into an edge-brightened toroidal geometry. The morphology of PKS B1400–33 does suggest such an interpretation if the torus is being viewed almost face on.

Extended halos are usually observed in clusters with a low spiral fraction, large velocity dispersion and high X-ray luminosity. These are the clusters that are expected to have merger histories and large scale shear and turbulence in the ICM and, consequently, halos. However, S753 is a poor cluster and, although it belongs to the Centaurus concentration of galaxies, it shows no evidence for subclustering (Willmer et al. 1991) or any anomalous distribution in the velocities of its members which might be indications of ongoing or past mergers.

As compared to other well studied halos and relic sources (Feretti 2002), PKS B1400–33 has a relatively small linear size and an extremely low radio luminosity. As discussed in section 6, the surface brightness of the source is extremely low, similar to that in cluster halos; however, the inferred p_e is more characteristic of cluster relics.

7.3. A relic of a lobe injected into the cluster environment?

The radio galaxy phenomenon, in which beams from an active nucleus power extended radio lobes, is believed to be short lived compared to the Hubble time. When the central engine switches off, presumably as the fuel is exhausted, the lobes suffer radiative losses that deplete the more energetic electrons and steepen the spectrum. However, expansion losses, if present, quickly render the synchrotron relic invisible because the radio power drops rapidly: in an expanding synchrotron bubble with a tangled magnetic field, the spectral luminosity falls as $L_\nu \sim f^{-(4\alpha+2)}$, where f is the expansion factor (Leahy 1991). For this reason, we expect invisible relics to be present in the intergalactic medium (IGM) where the ambient densities and gas pressures may be lowest, and relics may preferentially be visible in a higher density medium where expansion losses are smaller.

A plausible scenario for the origin of a cluster relic like PKS B1400–33 would be one in which activity in a galaxy located in the vicinity or boundaries of a cluster produced twin beams, of which one resulted in a radio lobe within the ICM and the other oppositely directed beam resulted in a second lobe outside of the cluster gas and in a relatively lower density IGM. The differences between the environments of the two lobes would be more pronounced if the double radio source is a giant radio source and the activity axis is aligned with a local gradient in the ambient gas density. Following cessation of nuclear activity in the host, the lobe in the IGM would quickly disappear from radio images, while the lobe located in the denser ICM would survive as a steep spectrum relic.

In this scenario, the extended source PKS B1400–33 would be one lobe of a relic double radio source. From the viewpoint of such an interpretation, the structure of the radio source (Fig. 1) suggests that the double may have been edge brightened and the NE rim of PKS B1400–33 (the region with the flattest spectral index) might be the site of past hotspots and the end of the double source. The low surface brightness filamentary emission trailing towards the SW from this rim could be the relic cocoon of the backflowing plasma. The overall spectral steepening observed from the NE rim towards the SW (see Fig. 6) is consistent with such a hypothesis. The faint protrusion past the rim along the SW boundary (marked P in Fig. 1) might be a relic bridge. We would expect a possible host galaxy to lie towards the SW and along the axis defined by the protrusion; a counterlobe, if it is detectable, may be located beyond that.

To test this hypothesis, we first searched wide-field NVSS and MOST images of this field for a possible counterlobe along the axis defined by the brightest portion of the NE arc and the SW protrusion in Fig. 1. A tentative MOST detection at 843 MHz was followed up with a pointed observation using the 23' field of view. When smoothed to a resolution of 2' FWHM, this observation gives marginal evidence for a very extended source (~ 50 arcmin 2)

with centroid position RA $13^h59^m30^s$, DEC $-34^\circ47'$ (J2000.0) and an integrated flux density of 50 ± 12 mJy. We then examined the optical field along the same axis for possible host galaxies. A candidate with $m_B = 16.7$, and classified as S0 by Willmer et al. (1991), was found at RA $14^h02^m18.3$, DEC $-34^\circ22'54''$ (J2000.0); it is marked H in Fig. 7. The peak of PKS B1400–33, the location of galaxy H and the peak of the extended source tentatively detected in the MOST observation are collinear within a few degrees.

We subsequently obtained an optical spectrum of galaxy H in the 4000–7700 Å window using the ANU 2.3-m telescope and double-beam spectrograph at Siding Spring Observatory in May 2002. Its redshift, $z = 0.01695 \pm 0.0002$, implies a peculiar velocity of 1090 km s^{-1} relative to the mean redshift of the cluster. Examining the distribution in galaxy velocities for a magnitude limited sample towards the cluster (see Fig. 4 in Willmer et al. (1991)), we infer that galaxy H is likely to be a member of S753. It lies $26'$ from the center of PKS B1400–33, implying a projected separation of $300h^{-1}$ kpc at the distance of the cluster. The optical spectrum shows narrow emission lines of H α , [N II] and the [S II] doublet; the [N II]/H α and [S II]/H α ratios are about 0.25 and 0.22 strongly suggestive of starburst activity (and not emission from an AGN environment).

AGN-type radio activity usually occurs in elliptical galaxies and the probability of such activity is an increasing function of optical luminosity. Samples of extended radio sources show a sharp decline for hosts with R -band optical luminosity $M_R \gtrsim -21$ (Ledlow 1997). On the other hand, in the cluster Abell 428, Ledlow, Owen and Keel (1998) do find a powerful extended radio source 0313–192 associated with an $M_B = -19.9$ disk-dominated host that is most likely an early type spiral (Sa–Sb). The argument against galaxy H being the host of PKS B1400–33 is simply that it is even further underluminous, with $M_B = -17.4$.

8. Summary

We have presented new and improved radio images of the relic source PKS B1400–33. We have discussed the origin of this relic in the light of recent progress in the understanding of relic synchrotron plasma in cluster environments. The diffuse source has an extremely low surface brightness and a steep spectrum, with radio properties unlike that of relics and halos observed in cluster environments. The unusual morphology, placement in the cluster and physical parameters indicate an unusual origin for this source.

The new data does not represent evidence suggesting that the relic source PKS B1400–33 was created by past activity in NGC 5419. Nor do the observations rule out this possibility. The discussions suggest that PKS B1400–33 is not a typical relic. The radio properties

suggest that if the source was created by processes similar to those that form the relics and halos, we might be observing an extreme form of a relic in a poor cluster environment or, perhaps, a relic of a re-energized relic. We have presented marginal evidence supportive of the hypothesis that the diffuse source PKS B1400–33 was born as a lobe of a powerful radio galaxy; however, we do not have a good candidate for the optical host. The source is unusual and the peculiar radio properties might be indicating an unusual origin: we favour the interpretation that the diffuse source is a relic of a lobe injected into the cluster environment as worthy of further consideration, particularly because of the novelty of the proposed phenomenon. Followup low frequency imaging of the field, possibly with the VLA at 74 MHz, with the aim of confirming the MOST detection of a counterlobe and better quality imaging of any low surface brightness connecting features, is proposed as the next step towards understanding the phenomenology in this unusual source.

The Australia Telescope Compact Array is part of the Australia telescope which is funded by the Commonwealth of Australia for operation as a National Facility managed by CSIRO. The National Radio Astronomy Observatory is a facility of the National Science Foundation operated under cooperative agreement by Associated Universities, Inc.

REFERENCES

Abell, G. O., Corwin, H. G., & Olowin, R. P. 1989, *ApJS*, 70, 1

Bird, C. M., Mushotzky, R. F., & Metzler, C. A. 1995, *ApJ*, 453, 40

Bolton, J. G., Gardner, F. F., & Mackey, M. B. 1964, *Aust. J. Phys.*, 17, 340

Brunetti, G., Setti, G., Feretti, L., & Giovannini, G. 2001, *MNRAS*, 320, 365

Churazov, E., Forman, W., Jones, C., & Böhringer, H. 2000, *A&A*, 356, 788

Churazov, E., Brüggen, M., Kaiser, C. R., Böhringer, H., & Forman, W. 2001, *ApJ*, 554, 261

Cotter, G. 1998, in *Observational Cosmology with the New Radio Surveys*, ed. M. N. Bremer, N. Jackson & I. Perez-Fournon, (Dordrecht: Kluwer), 233

Ensslin, T. A., Biermann, P. L., Klein, U., & Kohle, S. 1998, *A&A*, 332, 395

Ensslin, T. A., 1999, in *MPE Report 271, Diffuse Thermal and Relativistic Plasma in Galaxy Clusters*, ed. H. Böhringer, L. Feretti & P. Schuecker, (Garching: MPE), 275

Ensslin, T. A., & Brüggen, M. 2002, MNRAS, 331, 1011

Fabian, A. C., Sanders, J. S., Ettori, S., Taylor, G. B., Allen, S. W., Crawford, C. S., Iwasawa, K., Johnstone, R. M., & Ogle, P. M. 2000, MNRAS, 318, L65

Fadda, D., Girardi, M., Giuricin, G., Mardirossian, F., & Mezzetti, M. 1996, ApJ, 473, 670

Feretti, L., Perola, G. C., & Fanti, R. 1992, A&A, 265, 9

Feretti, L., & Giovannini, G. 1996, in Extragalactic radio sources, IAU Symp. 175, ed. R. Ekers, C. Fanti & L. Padrielli, (Dordrecht: Kluwer), 333

Feretti, L. 1999, in MPE Report 271, Diffuse Thermal and Relativistic Plasma in Galaxy Clusters, ed. H. Bohringer, L. Feretti & P. Schuecker, (Garching: MPE), 3

Feretti, L. 2002, in The universe at low radio frequencies, IAU Symp. 199, ed. V. K. Kapahi & A. P. Rao, (Dordrecht: Kluwer), astro-ph/0006379

Forman, W., Jones, C., Markevitch, M., Vikhlinin, A., & Churazov, E. 2002, in Astrophysics and Space Science Library 272, Merging Processes in Galaxy Clusters, (Dordrecht: Kluwer), 109

Giovannini, G., Feretti, L., Venturi, T., Kim, K. -T., & Kronberg, P. P. 1993, ApJ, 406, 399

Goss, W. M., McAdam, W. B., Wellington, K. J., & Ekers, R. D. 1987, MNRAS, 226, 979

Harris, D. E., Stern, C. P., Willis, A. G., & Dewdney, P. E. 1993, AJ, 105, 769

Kim, K. -T., Kronberg, P. P., Dewdney, P. E., & Landecker, T. L. 1990, ApJ, 355, 29

Ledlow, M. J. 1997, in ASP Conf. Ser. 116, The nature of Elliptical Galaxies; 2nd Stromlo Symposium, ed. M. Arnaboldi, G. G. Da Costa & P. Saha, 421

Ledlow, M. J., Owen, F. N., & Keel, W. C. 1998, ApJ, 495, 227

Leahy, J. P. 1991, in Cambridge Astrophysics Ser. 19, Beams and Jets in Astrophysics, ed. P. A. Hughes, (Cambridge: Cambridge Univ. Press), 100

Maia, M. A. G., da Costa, L. N., & Latham, D. W. 1989, ApJS, 69, 809

McNamara, B. R., Wise, M. W., Nulsen, P. E. J., David, L. P., Carilli, C. L., Sarazin, C. L., O'Dea, C. P., Houck, J., Donahue, M., Baum, S., Voit, M., O'Connell, R. W., & Koekemoer, A. 2001, ApJ, 562, L149

Miley, G. 1980, ARA&A, 18, 165

Mills, B. Y., Slee, O. B., & Hill, E. R. 1960, *Aust. J. Phys.*, 13, 676

Mulchaey, J. S., & Zabludoff, A. I. 1998, *ApJ*, 496, 73

Roettiger, K., Burns, J. O., Clarke, D. A., Christiansen, W. A., & Wayne, A. 1994, *ApJ*, 421, L23

Röttgering, H. J. A., Wieringa, M. H., Hunstead, R. W., & Ekers, R. D. 1997, *MNRAS*, 290, 577

Schuecker, P., & Böhringer, H. 1999, in MPE Report 271, Diffuse Thermal and Relativistic Plasma in Galaxy Clusters, ed. H. Böhringer, L. Feretti & P. Schuecker, (Garching: MPE), 43

Subrahmanyan, R., & Saripalli, L. 1993, *MNRAS*, 260, 908

Subrahmanyan, R., Saripalli, L., & Hunstead, R. W. 1996, *MNRAS*, 279, 257

Venturi, T., Bardelli, S., Zambelli, G., Morganti, R., & Hunstead, R. W. 1999, in MPE Report 271, Diffuse Thermal and Relativistic Plasma in Galaxy Clusters, ed. H. Böhringer, L. Feretti & P. Schuecker, (Garching: MPE), 27

Willmer, C. N. A., Focardi, P., Chan, R., Pellegrini, P. S., & da Costa, N. L. 1991, *AJ*, 101, 57

Table 1. Journal of observations.

Frequency (MHz)	Telescope	Epoch	Configuration
1398 and 2378	ATCA	1995 Jan	375m array
		1995 June	750B array
843	MOST	1998 May	23' f.o.v.
330	VLA	2000 March	CnB array
		2000 May, June	C array
		2000 July	DnC array

Table 2: Image parameters and total flux density of the extended source

Frequency (MHz)	Beam FWHM	Image r.m.s. noise (mJy beam ⁻¹)	Flux density (Jy)
330	77" × 53" at P.A. –24°	2.5	8.5
843	77" × 43" at P.A. 0°	1.0	1.3
1398	70" × 45" at P.A. 0°	0.5	0.46
2378	70" × 45" at P.A. 0°	0.5	0.10

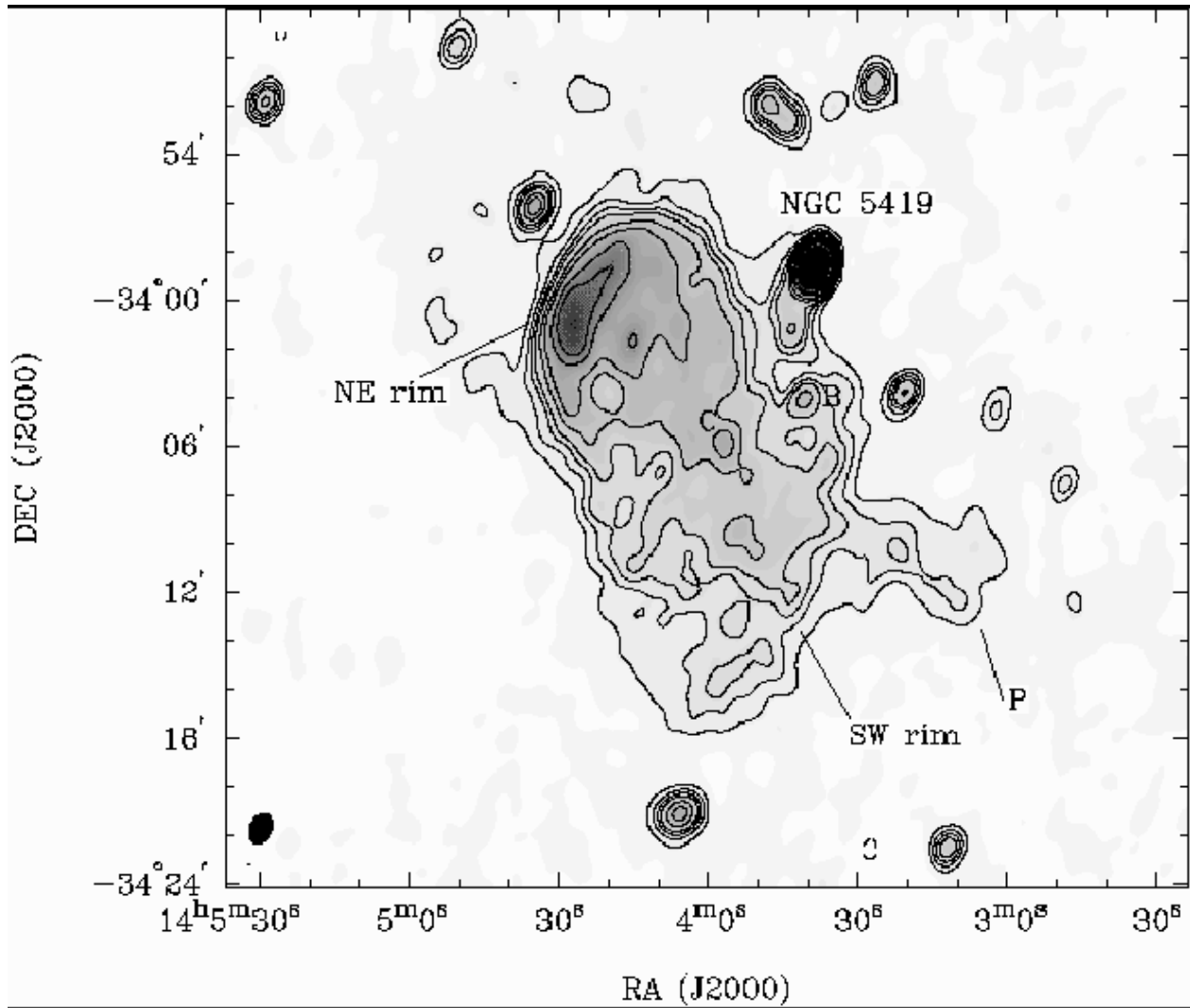


Fig. 1.— PKS B1400–33 at 330 MHz shown as a greyscale image with contours overlaid. The VLA image has been made with a beam of $77'' \times 53''$ at a P.A. of -24° ; contours are at $10 \text{ mJy beam}^{-1} \times (-1, 1, 2, 3, 4, 6, 8, 12, 16, 24, 32, 48, 64, 96, 128)$. The r.m.s. noise is about $2.5 \text{ mJy beam}^{-1}$ in source free regions. The NE rim, SW rim and protrusion towards the SW, which have been referred to in the text, have been labelled in the figure. This image, as well as all others displayed in this paper, has been corrected for the attenuation due to the primary beam; the shaded ellipses in the lower left corner of the images show the half-power size of the synthesized beams.

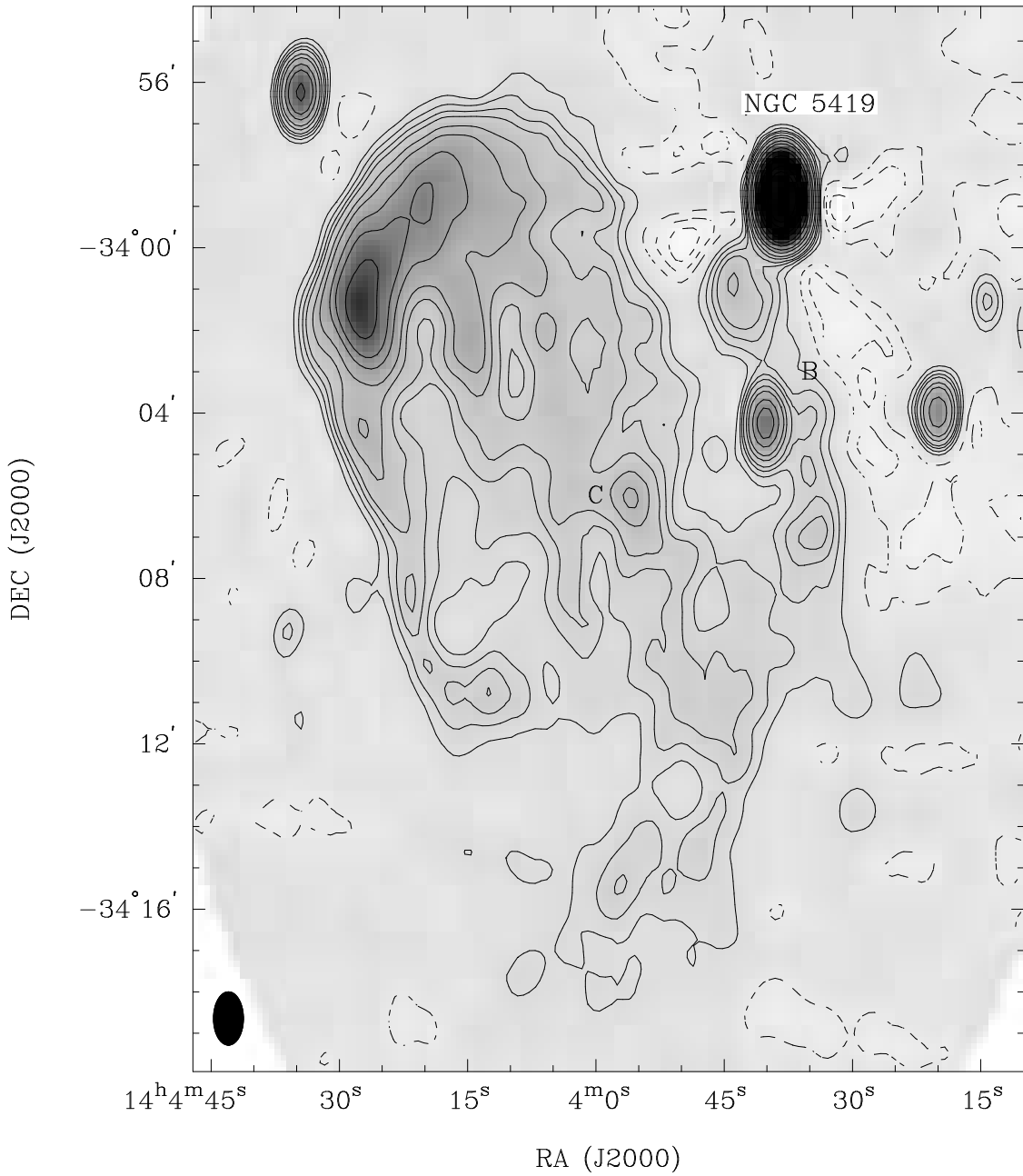


Fig. 2.— 843 MHz MOST image of PKS B1400–33 made with a beam of FWHM $77'' \times 43''$ at a P.A. of 0° . The image noise is 1 mJy beam^{-1} . Contours are at $2 \text{ mJy beam}^{-1} \times (-3, -2, -1, 1, 2, 3, 4, 6, 8, 12, 24, 32, 48, 64, 96, 128)$.

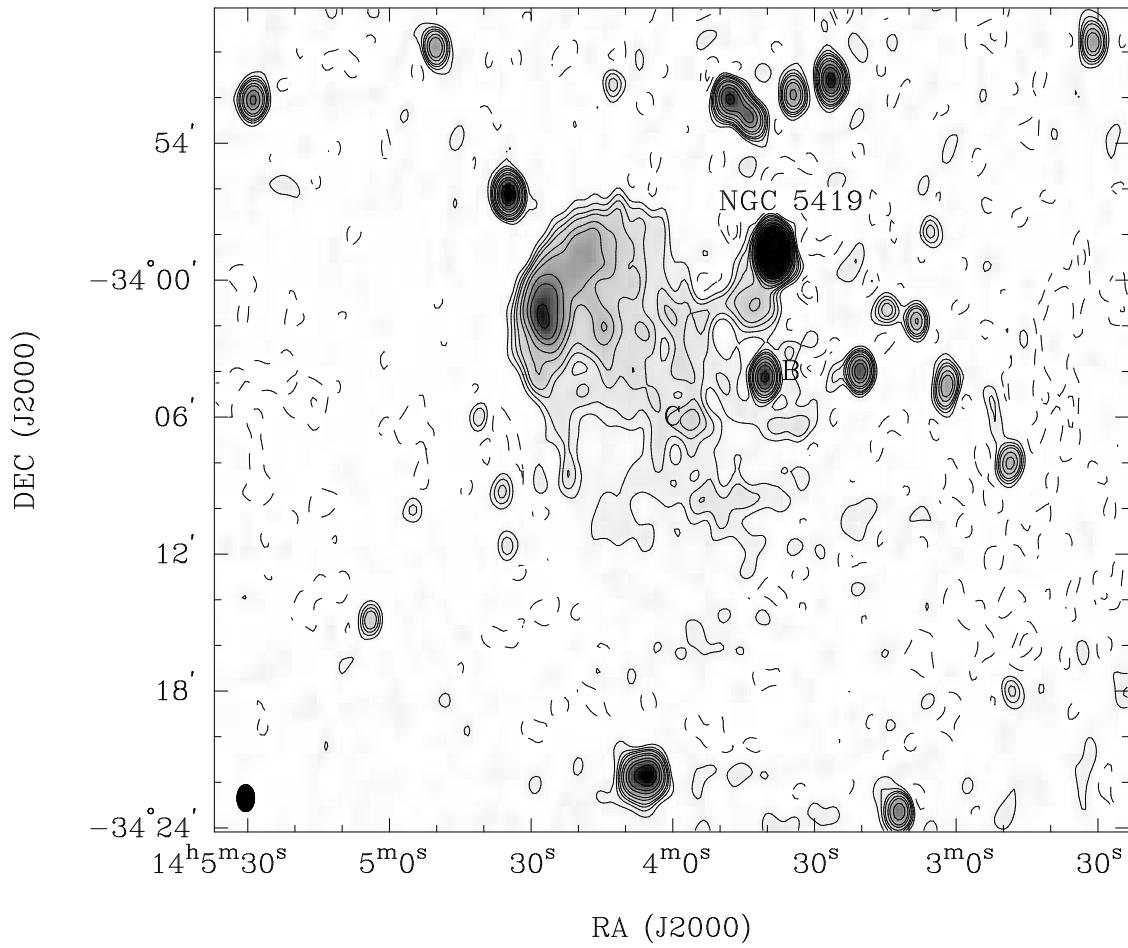


Fig. 3.— ATCA image of PKS B1400–33 made at 1398 MHz with a beam of FWHM $70'' \times 45''$ at a P.A. of 0° . The field was mosaic imaged with 9 pointing centers spaced $8'$ in RA and DEC. The image r.m.s. noise is 0.5 mJy beam $^{-1}$; contours are at $-3, -2, -1, 1, 2, 3, 4, 6, 8, 12, 24, 32, 48, 64, 96, 128$, and 192 mJy beam $^{-1}$.

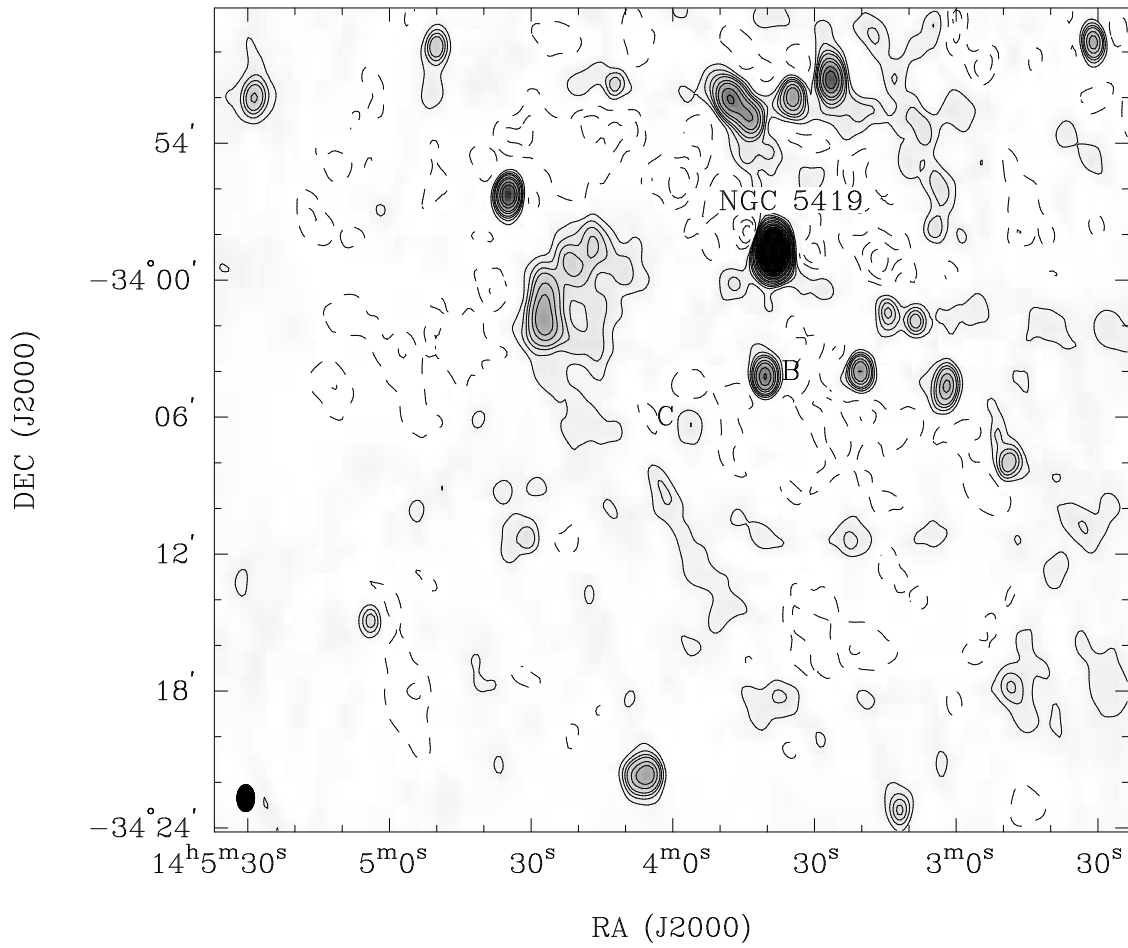


Fig. 4.— ATCA image of PKS B1400–33 made at 2378 MHz with a beam of FWHM $70'' \times 45''$ at a P.A. of 0° . The observations were made as a 9 pointing mosaic with fields spaced by $8'$ in RA and DEC. The image has an r.m.s. noise of $0.5 \text{ mJy beam}^{-1}$; contours are at $-3, -2, -1, 1, 2, 3, 4, 6, 8, 12, 24, 32, 48, 64, 96, 128$, and $192 \text{ mJy beam}^{-1}$.

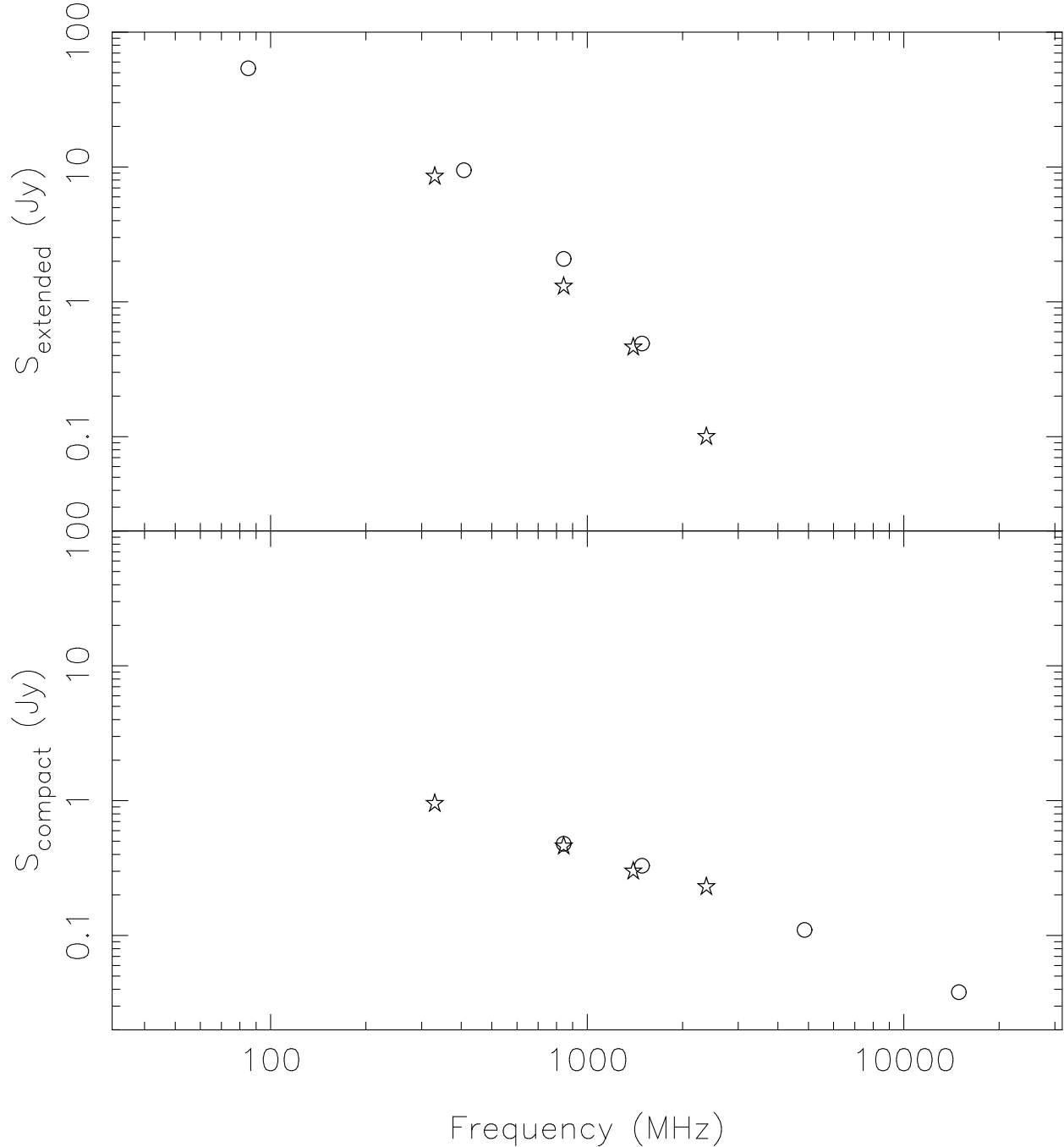


Fig. 5.— Radio spectra of the extended emission (upper panel) and the compact source associated with NGC 5419 (lower panel). The open circles represent previously published measurements, while the star symbols show flux density measurements derived from observations presented in this paper.

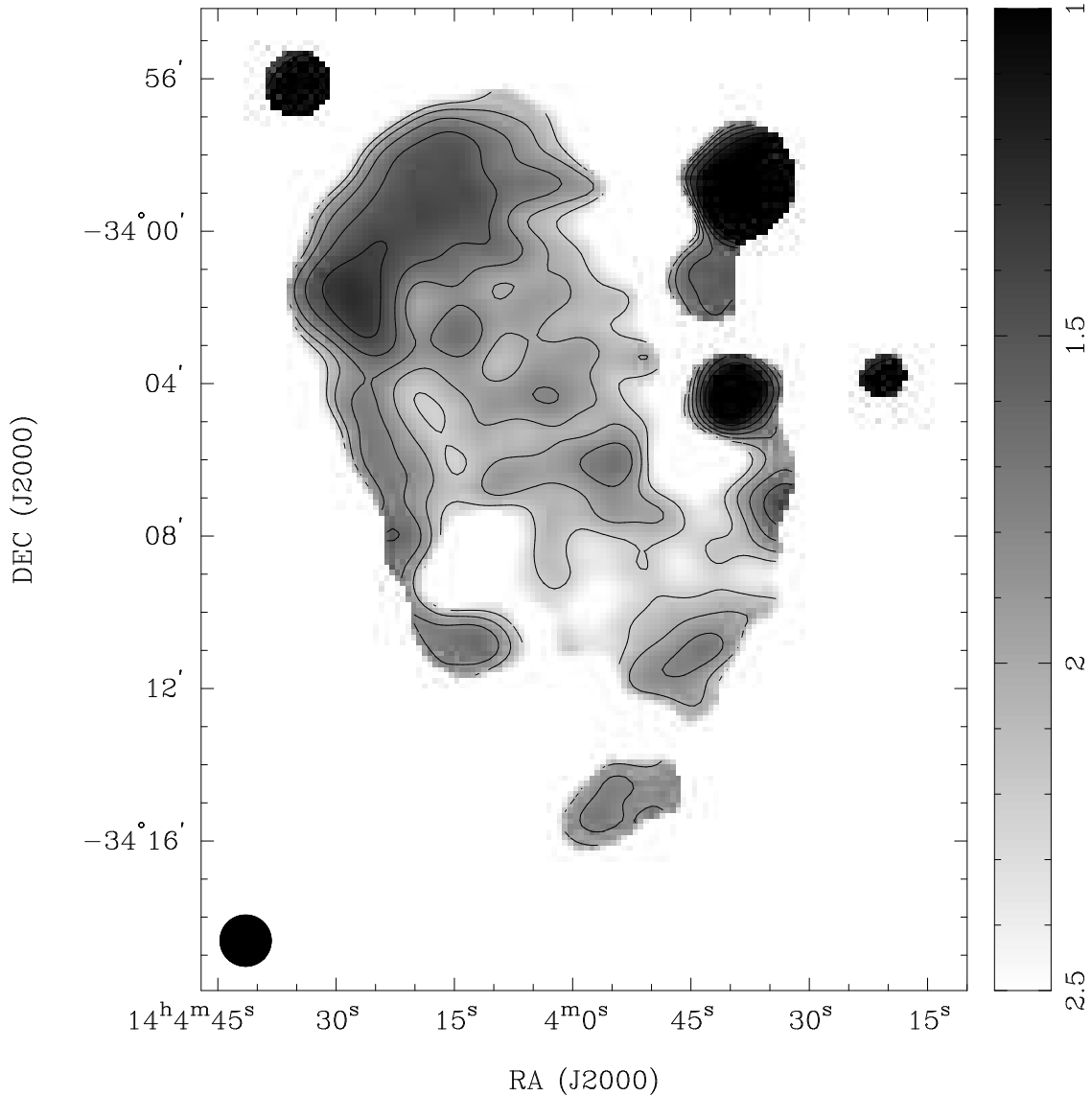


Fig. 6.— Distribution of the spectral index α between 330 and 843 MHz as computed from images made with a beam of FWHM $80''$. The $1 - \sigma$ uncertainty is ± 0.06 in α . Contours are at α values of 2.2, 2.0, 1.8, 1.6, 1.4, 1.2 and 1.0.

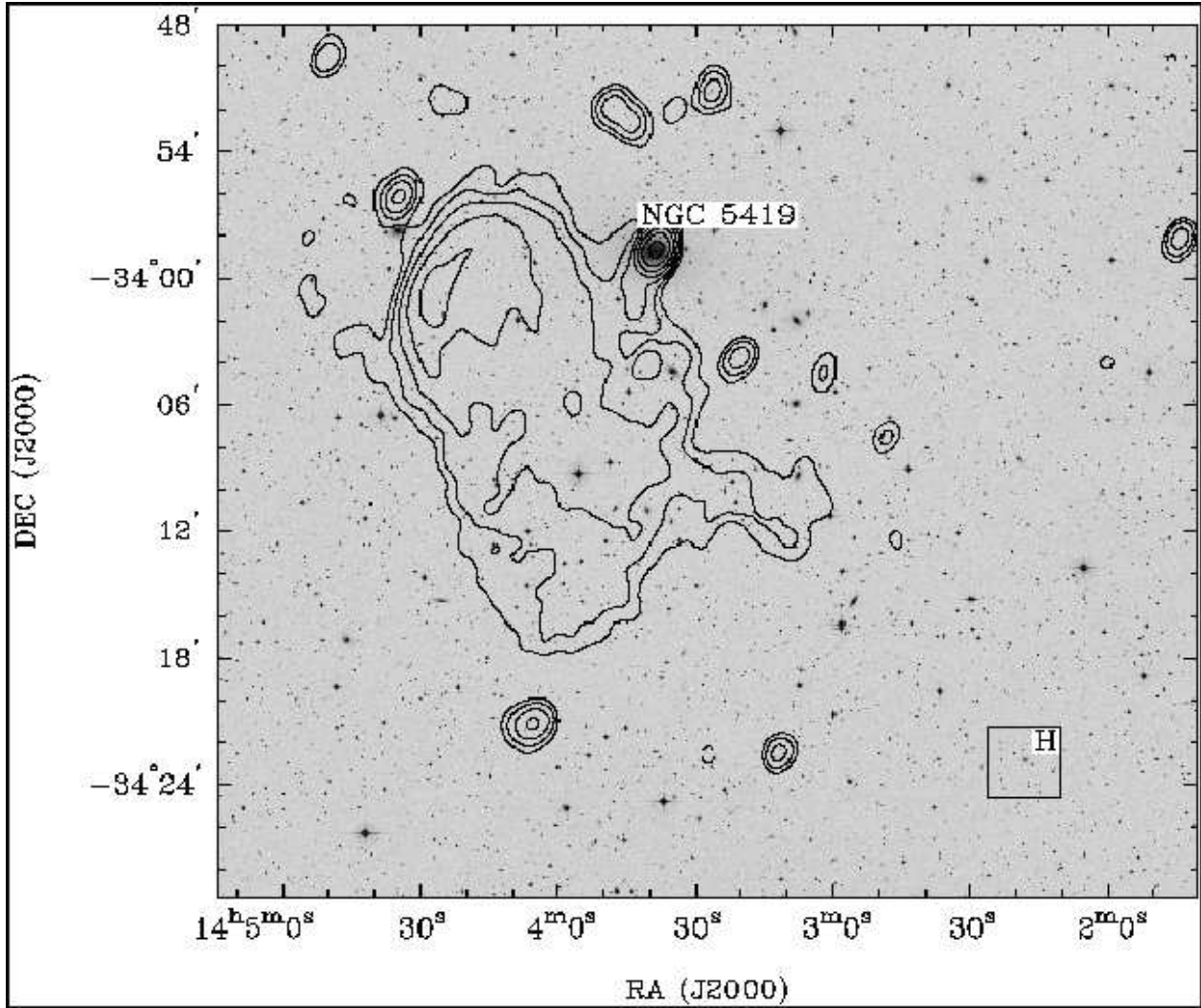


Fig. 7.— 330 MHz radio contours overlaid on a DSS digitization of the UK Schmidt SERC-J survey image of the field. Contours are at $10 \text{ mJy beam}^{-1} \times (-1, 1, 2, 4, 8, 16, 32, 64)$. The compact radio source identified with NGC 5419 is indicated; the candidate host galaxy discussed in section 7.3 is at the center of the box marked H.

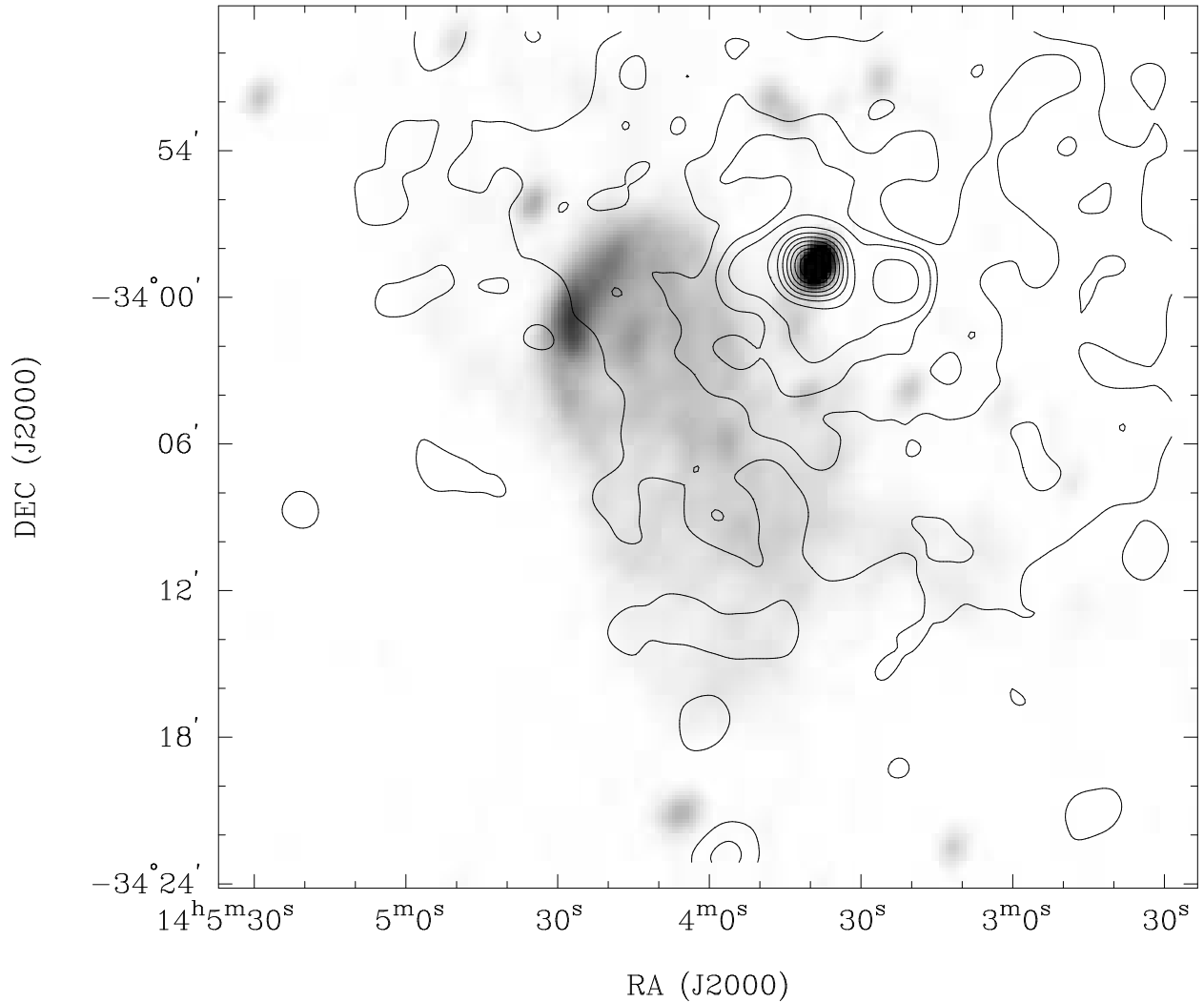


Fig. 8.— Contours of the ROSAT PSPC broad band X-ray image of the S753 cluster field overlaid on a greyscale representation of the 330 MHz VLA image shown in Fig. 1. The X-ray image has been smoothed to a resolution of 2.2 FWHM and the contours are at 8, 12, 16, 20, 30, 40, 50, 60, 70, 80 and 90 % of the peak.